Adaptive Damping Control of MMC to Suppress High-Frequency Resonance

Pengxiang Huang, *Student Member, IEEE*, and Luigi Vanfretti, *Senior Member, IEEE*

***Abstract*—High-frequency resonances (HFRs) between modular multilevel converters (MMCs) and power system are developed due to the delay-induced negative damping of MMCs. Because the resonance frequencies are unknown and dependent on the ac network configuration, system operating condition and MMC control modes, the efficacy of applying a predesigned damping control in advance is limited. To overcome this limitation, this paper presents an adaptive damping control scheme that employs online resonance detection to identify HFRs from voltage and current measurements and then automatically program narrowband damping control for the mitigation of HFRs. By continuously monitoring system resonance conditions (e.g., disappearance of resonance, frequency change of resonances, emergence of new resonances), it automatically adjusts the number of damping controllers being used, the value of damping gain for each damping controller, and the width of the damping band designed for each damping controller. The results of the Electromagnetic transient (EMT) simulation validate the effectiveness of the proposed method in different MMC-based systems.**

***Index Terms*—Modular multi-level converter, high-frequency resonance, active damping, narrowband damping, online resonance detection, adaptive control.**

I. Introduction

A. Motivation

HIGH frequency resonance (HFR) between an MMC and the external network may arise when the resonance frequency falls into the non-passive (i.e., negative damping) region of the MMC [1], which is caused by time delays. Delayed-induced negative damping has been found to occur periodically across a wide frequency range (e.g., from a few hundred Hz to the Nyquist frequency), possibly resulting in simultaneous resonances at multiple frequencies [2], [3]. Active filtering [4] and wideband damping can be effective within a specific frequency range. However, the phase shift introduced by both the time delay and the damping function usually exacerbates the negative damping of the MMC in the passband of the damping filter. This effect, in turn, makes MMC more prone to stability issues within that frequency range. Multi-tuned narrowband damping with phase-lead unit is thus preferred [2], as it can add positive damping to MMC at multiple pre-defined narrow ranges, and the phase-lead units can compensate the delay-generated phase shift on each single damping function [5]. Another difficulty in suppressing HFR arises from the sensitivity of the resonance frequency to variations in the ac network configuration, system operating conditions and MMC control modes. As such, these HFR conditions cannot be predicted off-line, nor effectively mitigated by designing a fixed damping control in advance, whether wideband or narrowband damping methods. To overcome this issue, a narrowband damping function can be employed in conjunction with online stability monitoring methods. Such combination effectively identifies HFR first and then narrowly suppresses it in real time, namely adaptive narrowband damping.

B. Literature Review

The implementation of adaptive narrowband damping necessitates the precise estimation of the resonance frequency with minimal latency. This requirement stems from two crucial factors: first, inaccurate estimations can lead to damping control being applied to the wrong frequency range, thereby degrading effectiveness of damping control; second, delays in detecting and suppressing high-frequency resonance components could trigger relay tripping, because the unstable oscillating current or voltage can exceed protective thresholds within a mere few tens of milliseconds, or even less.

There are two primary methods for identifying system resonance frequencies: online impedance measurement-based method [3], [6], and online resonance detection-based method [5], [7], [8]. The former involves measuring the ac network impedance through active perturbations into the network, followed by determining the resonance frequencies via comparing the network impedance to the MMC impedance using the Nyquist stability criterion. However, the online impedance measurement-based methods fail to meet the aforementioned requirement on estimating resonance frequency. In addition, this approach is often plagued by the problem of a large computation burden and is susceptible to frequency spectrum distortions due to improper perturbation signal design (e.g., low immunity to noises and background harmonics, especially when the energy of the injection signal is distributed over a wide frequency range). Consequently, the online impedance measurement-based method is ineffective for adaptive damping of HFRs.

The second approach generally consists of two stages: 1) direct monitoring on oscillations in the voltages and currents of an MMC, which is an indication of potential system resonances; and 2) characterizing oscillatory signals at different frequencies, and distinguishing between components associated with system resonances and other types of components that are not related to resonances (e.g., electrical transients and background harmonics). Fourier analysis-based methods, as detailed in [5], [7], [8], is widely adopted in the first stage. For prompt and accurate estimation of oscillatory components' frequencies in the high-frequency (HF) range, [5] adopts the windowed three-point interpolated Discrete Fourier Transform

(IpDFT), which is a method widely used for synchrophasor estimation [9], [10] to reduce reporting latency and minimize spectral leakage. In the second stage, to identify the resonance, [7] employs an amplitude threshold-based approach. Specifically, by using Fourier analysis, a component is identified as resonance once its amplitude exceeding a predetermined threshold. Recognizing that electrical transients can potentially cause false detection when using amplitude threshold, [8] incorporates an additional frequency threshold alongside the amplitude threshold. Consequently, only frequency spectrum components above the pre-defined frequency will be identified as resonances. One of the main challenges of these threshold-based identification methods is the determination of a suitable threshold value. If the amplitude-threshold is set too high, the method might not promptly detecting slow-growing resonances that could still affect the system performance until they are exceeding threshold and identified. If set too low, it could lead to false positives, identifying fluctuating background harmonics and system noise as resonances. In addition, the optimal amplitude-threshold value can vary depending on the configuration of the ac network and the operating conditions of the system. A static threshold might not work effectively under all resonance conditions, and case-by-case adjustments of the threshold to align with changing conditions are impractical. On the other hand, the frequency threshold is often determined based on the actual frequency range of HFR events [8] from experience, which may also vary on a case-by-case basis. Given the limitations of the threshold-based resonance identification method utilized in [7], [8], a more reliable identification method is needed.

Once the resonance is detected, its frequency and amplitude are used to guide the design of narrowband damping controls. In [7], a single-tuned narrowband damping controller is used to suppress a single resonance between an inverter and the grid, however, both the bandwidth of the bandpass filter and the damping gain cannot be adjusted according to the resonance conditions of the system. Meanwhile, [11], [12] present a method for adaptive gain tuning through a PI compensator, which gives the minimum amount of gain needed to damp the system resonance. However, this may result in a change in the resonance frequency after the damping control is applied, and therefore, should be avoided especially in damping multiple HFRs. To suppress multiple HFRs of MMC associated with time delay, adaptive notch filters (ANFs) have been used to remove the time delay effect that is subjected by MMC under multiple detected resonance frequencies [8]. However, [8] assumes that the multiple HFRs appear consecutively, in other words, at a single frequency at a time. Additionally, ANFs-based damping control lacks the capability of providing extra amount of damping needed by MMC. As a result, depending on the inherent resistance of the ac network, ANFs-based damping method could lead to under-damped or marginally damped resonances, resulting in a relatively long decay time.

To address the above-mentioned problems, this paper introduces a novel adaptive damping control scheme for the detection and mitigation of MMC HFRs, particularly under conditions of multiple co-existing HFRs and varying grid circumstances. To overcome the limitations of threshold-based resonance identification methods, a rate-of-change (ROC)-based resonance identification method is proposed, which ensures reliable and precise discrimination of system resonances from other unrelated oscillatory signals. Upon the identification of HFRs, an adaptive damping design method is proposed to automatically design and employ multi-tuned damping control to mitigate multiple detected resonances. Specifically, a multi-tuned damping control design is applied to obtain the initial damping gains for the dampers at different detected resonance frequencies. These gains are then further adjusted on the basis of continuous monitoring of the system resonance conditions. Moreover, this paper presents an adaptive tuning rule for the bandwidth of the damping controller and also a method to identify disappeared resonances and to deactivate corresponding damping controls.

C. Contributions

The specific contributions of this paper are:

- Introducing a ROC-based resonance identification method to overcome the limitations of threshold-based resonance identification methods.
- Presenting an automatic design method for the multi-tuned damping control of MMC after the identification of multiple HFRs.
- Proposing an adaptive gain adjustment method for the designed multi-tuned damping controller.
- Proposing an adaptive tuning rule for the bandwidth of the damping controller.
- Proposing a method for identifying disappeared resonances and deactivating corresponding damping controls

D. Organization

The reminder of this paper is organized as follows. Section II describes the system under study and the narrowband damping control effect. Section III reviews the multi-tuned narrowband damping control using ac voltage feedforward, which is used in the proposed adaptive damping control scheme in the sequel. Section IV introduces an online resonance detection algorithms developed to accurately identify the HFRs. Section V proposes the automatic method for conducting multi-tuned damping controls based on detected resonances, along with the discussion on related adaptation rules of damping controls and the deactivation of damping controls at frequencies where early detected resonances have disappeared. EMT Simulations to illustrate the effectiveness of the proposed adaptive damping control and the advantages of it when compared to other existing methods in the literature are shown in Section VI. Section VII concludes the work.

II. System and MMC Damping Control

A. System Description and Simplified MMC Impedance Model

Fig. 1 depicts a single-line diagram of an MMC connected to an external ac network through a transformer. The figure also shows the structure of proposed adaptive damping control, demonstrating that it is placed in parallel with the MMC's main controllers. The adaptive control includes two parts: (1)

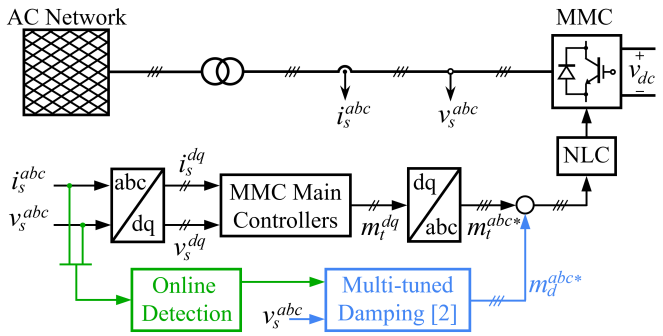

Fig. 1. Circuit diagram and control structure of MMC with adaptive damping control.

online resonance detection unit, and (2) multi-tuned narrowband damping function exploiting voltage feedforward. As this paper focuses on suppressing resonances of MMC in HF range, the HF impedance model developed in [2] for MMC can be adopted for use here, in which those MMC controls whose effects diminish at this frequency range can be neglected [2], [13], [14]. This implies that the phase-locked loop, circuiting current control and energy controls are all omitted from HF impedance model. In addition, due to the low bandwidth of the dc-bus voltage regulator and the slow dynamics of the submodule capacitors, constant dc-bus voltage is assumed. As a result, the impedance model of MMC in HF range can be described by:

$$Z_p(s) = \frac{R_{eq} + sL_{eq} + e^{-sT_d}G_c(s)}{1 + e^{-sT_d}(s)G_v(s)} = \frac{N_p(s)}{D_p(s)} = \frac{1}{Y_p(s)} \tag{1}$$

where $(R_{eq} + sL_{eq})$ represents half of the arm impedance, and e^{-sT_d} accounts for the time delay effect. $N_p(s)$ and $D_p(s)$ represent the numerator and denominator of $Z_p(s)$ respectively. $G_c(s)$ and $G_v(s)$ represent regulators related to ac current and ac voltage whose effect on an MMC retains at high frequencies. Note that, $G_c(s)$ and $G_v(s)$ come in different forms depending on the control modes of MMC, which are summarized in Table I of [2].

The ac network in Fig. 1 refers to the system that the MMC connects to, which can be classified into two types by considering the phase characteristics of its equivalent impedance (marked as $Z_g(s)$):

- Passive network, mainly comprised of overhead transmission lines, cables or parallel/series compensation units. Although it includes mainly passive elements, $Z_g(s)$ has a relatively small degree of passivity in a wide frequency range due to the small amount of inherent line resistance.
- Active network dominated by power converters, such as those in photovoltaic farms, wind farms, and battery energy storage systems. In such networks, $Z_g(s)$ inevitably exhibits negative damping in certain frequency ranges due to the control characteristics of the power converters (e.g., PLL-related negative damping in the low frequency range, delay-induced negative damping in the HF range).

The positive net-damping stability criteria [15], states that the stability of the MMC against the external network is guaranteed if the net-impedance is passive, indicating $\Re\mathfrak{e}\{Z_p(s) + Z_g(s)\} > 0$. Therefore, the damping control should be able to provide additional damping to compensate for the negative damping introduced by the ac network besides merely compensating the negative damping of the MMC.

B. Voltage Feedforward Damping Effect

As can be seen in Fig. 1, the voltage feedforward damping controller is placed in parallel with the main controllers of MMC (e.g., $G_c(s)$ or $G_v(s)$), and the control output is sent directly to the modulator. Thus, the damping effect is equivalent to adding $e^{-sT_d}H_d(s)/N_p(s)$ to $Y_p(s)$, where $H_d(s)$ represents the transfer function of the damping controller. The admittance of the MMC with a voltage feedforward damping scheme is given by:

$$Y_{pd}(s) = \frac{1 + e^{-sT_d}\left[H_d(s) + G_v(s)\right]}{R_{eq} + sL_{eq} + e^{-sT_d}G_c(s)} = Y_p(s) + \overbrace{\frac{e^{-sT_d}H_d(s)}{N_p(s)}}^{Y_r(s)} \tag{2}$$

with the subscript *pd* indicating the MMC impedance damped by voltage feedforward damping. As indicated by (2), the voltage feedforward damping can be viewed as introducing a virtual admittance $Y_r(s)$ in parallel with the undamped MMC admittance $Y_p(s)$. Therefore, if $Y_r(s)$ can be designed to be real positive valued at resonance frequency f_r (i.e., $Y_r(j2\pi f_r) = |Y_r(j2\pi f_r)|\angle\varphi$ with augment $\varphi = 0$), the negative net-damping can be compensated. However, the damping effect of $Y_r(s)$ needs to be limited to a pre-defined frequency range around f_r by using a bandpass filter (centered at f_r) in $H_d(s)$, in order to avoid unintended effects at other frequencies [2].

III. Narrowband Damping

A. Damping Control Function $H_d(s)$

The first-order complex coefficient filter (CCF) is adopted to limit the damping function $H_d(s)$ to a desired frequency range and is given by:

$$H_{ccf}(s) = \frac{\omega_b}{s - j\omega_r + \omega_b} \tag{3}$$

where ω_r and ω_b represents the center frequency and cutoff frequency of CCF in rad/s.

To ensure the narrowband damping adds a virtual positive conductance at the resonance frequency f_r, it is necessary to compensate for all potential phase lags posed upon $Y_r(s)$ at f_r. As evident in (2), both e^{-sT_d} and $N_p(s)$ introduce phase lags to $Y_r(s)$. To compensate for such phase lags, a steady-state phase-lead compensation $e^{j\theta}$ can be included in $H_d(s)$, and θ is selected to be $-\angle e^{-j2\pi f_r T_d}/N_p(j2\pi f_r)$.

In this section, we only elaborate on the multi-tuned damping function via multiple parallel CCFs (MCCF) due to the fact that a single resonance can be regarded as a special case of multiple resonances. Assume that the multiple resonance frequencies are $f_{r1}, f_{r2}, ..., f_{rn}$, the multi-tuned damping function $H_d(s)$ is given by:

$$H_d(s) = \sum_{k=1}^{n} K_{dk}e^{j\theta_k}H_{ccfk}(s) = \sum_{k=1}^{n} \frac{K_{dk}e^{j\theta_k}\omega_{bk}}{s - j\omega_{rk} + \omega_{bk}} \tag{4}$$

where $\omega_{rk}|_{k=1,...,n}$ and $\omega_{bk}|_{k=1,...,n}$ determines the center frequency and bandwidth of the n used CCF respectively, and $K_{dk}|_{k=1,...,n}$ is the designed damping gains for the n CCFs.

B. Design of Damping Gains

To prevent that the detected resonance frequency drifs out of the damping band after applying the multi-tuned damping controllers, the magnitude of the MMC admittance at each resonance frequency $f_{rk}|_{k=1,...,n}$ should be kept as constant as possible before and after applying the damping controllers. Hence, the damping gain for the virtual admittance at f_{rk} should be calculated by:

$$K_{dk} = \frac{x_k \left|\mathfrak{Re}\left\{Y_p(j2\pi f_{rk})\right\}\right|}{Y_{dk}(j2\pi f_{rk})} - \frac{\left|\sum_{j=1,j\neq k}^{n} K_{dj}\mathfrak{Re}\left\{Y_{dj}(j2\pi f_{rk})\right\}\right|}{Y_{dk}(j2\pi f_{rk})} \tag{5}$$

$$Y_{dk}(j2\pi f_{rk}) = \frac{e^{j\theta_k}e^{-sT_d}H_{ccfk}(j2\pi f_{rk})}{N_p(j2\pi f_{rk})} \tag{6}$$

where H_{ccfk} has the form shown in (3), x_k expresses the desired amount of positive conductance (i.e., $\mathfrak{Re}\{Y_r(j2\pi f_{rk})\}$) in terms of a base quantity selected as the conductance of the "undamped" MMC (i.e., $\mathfrak{Re}\left\{Y_p(j2\pi f_{rk})\right\}$), with per-unit values (p.u.). As can be seen in (5), the solution of the damping gain K_{dk} at f_{rk} is cross-coupled with the damping gains at other resonance frequencies. As a result, the damping gain for each damping function must be designed simultaneously. The damping gain vector $\boldsymbol{K}_d = [K_{d1}, K_{d2}, ..., K_{dn}]^{\mathrm{T}}$ is calculated by solving:

$$\boldsymbol{K}_d = \begin{bmatrix} \mathfrak{Re}\{\mathbf{Y}_{dk}(j\omega_{r1})\} \\ \mathfrak{Re}\{\mathbf{Y}_{dk}(j\omega_{r2})\} \\ \vdots \\ \mathfrak{Re}\{\mathbf{Y}_{dk}(j\omega_{rn})\} \end{bmatrix}^{-1} \cdot \mathrm{diag}(x_k) \cdot \begin{bmatrix} \mathfrak{Re}\left\{Y_p(j\omega_{r1})\right\} \\ \mathfrak{Re}\left\{Y_p(j\omega_{r2})\right\} \\ \vdots \\ \mathfrak{Re}\left\{Y_p(j\omega_{rn})\right\} \end{bmatrix} \tag{7}$$

where, $k = 1, 2, ..., n$ and $\omega_{rk} = 2\pi f_{rk}$. $\mathbf{Y}_{dk}(j\omega_{rk})$ are essentially row vectors with n entries, which represent the amount of conductance at f_{rk} provided by each virtual admittance "unit" at f_{rk}. Each element in $\mathbf{Y}_{dk}$ has the same form as $Y_d(s)$ in (6). Note that, in general, the entry in $\mathrm{diag}(x_k)$ can be determined considering damping requirements, such as system stability margins. However, when the design of the virtual admittance is adapted using online resonance detection, x_k is set to 2 as the starting point for the adjustment of x_k. Further adjustment of x_k should be based on a continuous evaluation of the MMC current (or voltage) behavior after applying the damping controller, which will be discussed in Section IV. Readers are referred to [2] for more comprehensive explanation of the multi-tuned damping control.

Equation (7) can be written in a shortened form as:

$$\boldsymbol{K}_d = \mathbb{Y}^{-1}\mathbb{X}\boldsymbol{b} \tag{8}$$

which highlights an important feature of this multi-tuned damping design procedure: it can be easily solved using linear algebra in computing resources, making it suitable for online adaptive control.

IV. Online Resonance Detection

Generally, resonance can be divided into unstable and sustained resonances, based on the oscillatory behavior of signals associated with the resonances (i.e., growing and unbounded, or stable). In the case of an MMC connected to an external system, the two types of resonances can be attributed to the negative and zero net-damping at the frequency of the system resonance, respectively. In this section, we present the detection method for locating both types of resonance with unknown frequencies.

A. Frequency and Magnitude Estimation of Spectral-Peaks

Spectral-peaks are the prominent components in a spectrum and are sometimes referred to as maximum-amplitude components [16]. A spectral peak above a certain threshold in an electrical power system, aside from the fundamental frequency component of the system, could potentially indicate a resonance. Hence, it is crucial to have a mechanism in place to extract the spectral-peak and estimates its frequency and amplitude, prior to the characterization of it.

1) Fourier Analysis of Measurement Data

To meet the requirements on low reporting latency (i.e., short response time), the short-time Fourier transform (STFT) is applied to the MMC current (or voltage) to obtain its frequency spectrum. This implies computing the fast Fourier transform (FFT) for a succession of windowed measurements, where the window "hops" forward through time. As the focus of the paper is to detect and damp the resonance above 2^{nd}-order harmonic frequency, several considerations must be made when applying the STFT:

- Choice of window length: To avoid spectral leakage of the fundamental frequency component at f_1, the window length shall correspond to one fundamental cycle or multiples thereof.
- Determination of the fundamental frequency f_1: Ideally, f_1 is chosen as a fixed value determined by the rated fundamental frequency of the power system (that is, 50 or 60 Hz). However, to avoid fundamental frequency fluctuation-related spectral aliasing, f_1 should be determined using a frequency locked loop (FLL).
- Choice of hop size (N_{hop}) of time window: To attain a good trade-off between accuracy and computational cost/time, the volume of measurement data used should be at least sufficient to monitor the behavior of a certain spectral-peak signal over a total time span exceeding 50 *ms*. This is because most transient signals below 5 kHz disappear within 50 *ms*. As an example, if one want to characterize a spectral-peak by using three windows of measurement, N_{hop} should be chosen based on the equation $(3N - 2N_{hop})/f_s \geq 50$ *ms*, where f_s is the sampling frequency and N is the number of samples per window.
- Choice of windowing function: a Hanning window function is used to mitigate spectral leakage.

2) Fourier Spectrum in Sequence Domain

It is worth noting that in a three-phase power system, the STFT should be applied concurrently to measurement data from three phases to obtain the Fourier spectrum of signal in each individual phase. As the system stability is assessed by impedance-based stability criterion in sequence domain and the corresponding damping control design also involves knowledge of the actual sequence domain where the spectral peak is present, the three-phase frequency spectrums should be transformed into positive and negative sequences. This transformation can be accomplished through symmetrical component analysis, as detailed below

$$\begin{bmatrix} X_{wp}(k) \\ X_{wn}(k) \end{bmatrix} = \frac{1}{3} \begin{bmatrix} 1 & \mathbf{a} & \mathbf{a}^2 \\ 1 & \mathbf{a}^2 & \mathbf{a} \end{bmatrix} \begin{bmatrix} X_{wa}(k) \\ X_{wb}(k) \\ X_{wc}(k) \end{bmatrix} \tag{9}$$

where the $\mathbf{a} = e^{j\frac{2\pi}{3}}$; the subscript wa, wb and wc represent the Hanning-windowed component in phase a, b and c respectively; the subscript p, n represent the Hanning-windowed positive and negative sequence component.

After obtaining frequency spectrum in sequence domain, spectral-peak identification is then performed in three steps:

- The first step is to determine the frequency regions of interest. For this work, the frequency range from 100 Hz up to the Nyquist frequency is examined. In practical applications, this range can be narrowed based on prior knowledge and past experiences of where resonances are likely to occur.
- The second step involves searching for local maxima in the magnitude spectrum, which are then deemed as spectral peaks.
- The third step is to refine the frequency and magnitude estimations for the identified spectral peaks, a process which is explained in further detail later in this text.

3) Refine the Estimation by Interpolated FFT

Since the detected resonance frequency will be the center frequency that CCF synthesized to, it is imperative to estimate the frequency as accurately as possible. When using STFT, a well-known tradeoff exists between the length of time window needed to truncate measurement, the number of data points collected in each window, the type of time-domain window used, and the spectral resolution that can be achieved in the frequency domain. As an example, if the time window contains measurements from two fundamental cycles (i.e., 0.04 s), the frequency resolution of the spectrum is 25 Hz. In the case of HFR is not at integral multiples of 25 Hz, the estimation of its frequency may be inaccurate. In order to solve this problem, an interpolation algorithm based on three FFT bins around spectral peak bin k_m (i.e., $X_w(k'_m-1)$, $X_w(k'_m)$, and $X_w(k'_m+1)$) is adopted to correct the estimation of frequency and amplitude. The equation for the IpDFT is given by

$$\begin{cases} \delta_m = 2\frac{|X_w(k'_m+1)|-|X_w(k'_m-1)|}{|X_w(k'_m+1)|+2|X_w(k'_m)|+|X_w(k'_m-1)|} \\ f_m = (k'_m+\delta_m)\Delta f; \quad \varphi_m = \angle X_w(k'_m) - \pi\delta_m \\ A_m = |X_w(k'_m)|\left|\frac{\pi\delta_m}{\sin(\pi\delta_m)}\right|\left|\delta_m^2-1\right| \end{cases} \tag{10}$$

where δ_m the displacement bin frequency; f_m, A_m, φ_m the refined frequency, amplitude and phase angle of the highest DFT bin above 2^{nd}-order harmonic frequency.

B. Identification of Resonance

Let estimated amplitude of the spectral-peak at f_m^0 be denoted as $A^0(f_m^0)$, where the subscript 'm' represents the maximum-amplitude component (i.e., spectral-peak), while the superscript '0' indicates the spectrum calculated from the most recent measurement window. Now, let the superscript '$-j$' indicate the spectrum calculated from j^{th} previous measurement window, while positive 'j' indicate the spectrum calculated from j^{th} future measurement window. $A^0(f_m^0)$ is then compared with a preset threshold value A_{th} (normally 1% to 5% of the MMC rated current or voltage at fundamental frequency). Note that most resonance identification algorithms determine the resonance by comparing the spectral peak over a certain threshold. However, observe that amplitudes above A_{th} are not always indicative of real resonances as some sources of electrical transients can temporarily produce high amplitude spikes. Consequently, to further characterize the spectral-peak and set apart a "real" resonance from other co-existing disturbance, **Algorithm 1** is proposed in this subsection, which can be divided into the following two parts, as follows.

Algorithm 1 Identification of the Resonance

Input: 1) f_m^0; 2) $A^0(f_m^0)$, $A^1(f_m^0)$ and $A^2(f_m^0)$; 3)$\overrightarrow{F_{rn}} = (f_{r1}, f_{r2}, ..., f_{rn})$;
Output: 1) $\overrightarrow{F_r} = (f_{r1}, f_{r2}, ..., f_{rn}, f_{rk})$; 2) $E_n(f_{rk})$
1: **if** $A^2(f_m^0) < A^1(f_m^0) < A^0(f_m^0)$ **then** $\overrightarrow{F_r}$=$\overrightarrow{F_{rn}}$; $E_n(f_{rk})$=0;
2: **else**
3: **for** $j = 1, 2, 3, \ldots, q-1$ **do**
4: **if** $A^{-j}(f_m^0) < A_{th}$ **then** $\overrightarrow{F_r}$=$\overrightarrow{F_{rn}}$; $E_n(f_{rk}) = 0$;
5: **else**
6: **if** $f_m^{-(q-1)} = f_m^{-(q-2)} = ... = f_m^{-1} = f_m^0$ **then**
7: $k =$ **sizeof**$(\overrightarrow{F_{rn}}) + 1$, $\overrightarrow{F_r}(k) = f_m^0$, $f_{rk} = f_m^0$,
8: $E_n(f_{rk}) = 1$

1) Distinguish Transient from Resonance (Line 1)

Considering the majority of transient signals below 5 kHz disappear within 50 ms [17], a simple identification method is to continuously monitor how the spectral-peak frequency bin in the most updated spectrum behaves in the next few sets of windowed measurements. If the amplitude of this spectral-peak component gradually decays, despite exceeding A_{th} in few consecutive windows, the MMC just needs to ride through it until it disappears. For example, after observing $A^0(f_m^0)$ at frequency f_m^0 is greater than A_{th}, we first extract amplitudes of component at f_m^0 in the next two fundamental cycles, which are denoted as $A^1(f_m^0)$ and $A^2(f_m^0)$. The component will be regarded as a transient signal, and the narrowband damping control will not be applied, if $A^2(f_m^0) < A^1(f_m^0) < A^0(f_m^0)$. Note that, $A^1(f_m^0)$ and $A^2(f_m^0)$ may not be spectral peaks in their measurement windows.

2) Determination of Resonance (Line $2 \sim 7$)

Once it is established that the spectral peak at f_m^0 is not attributed to a transient oscillation, the second part of the resonance identification starts by determining whether the spectral-peaks in the previous (q-1) windows are all correspond to frequency f_m^0 (line $2 \sim 4$). In the case that all the spectral peaks in the (q-1) windows are at f_m^0, the proposed algorithm will further check whether the magnitudes of these spectral-peaks are all larger than A_{th} (line 6). If so, f_m^0 is stored in a vector $\overrightarrow{F_{rn}}$ with all other resonance frequencies detected earlier and an enabling signal $E_n(f_{rk})$ is sent to the next stage to parameterize the multi-tuned narrowband damping including CCF centerred at f_{rk}(line $7 \sim 8$).

V. Adaptive Damping Control for Suppressing Multiple Resonances

A. Damping Design Scheme for Multiple Resonances

Expanding from the narrowband damping approach proposed in [2], the proposed damping scheme is defined as follows: once a dominant resonance is detected, a narrowband damping controller is automatically applied to the detected resonance frequency to suppress it. Then, such a process can be repeated to detect the 2^{nd}, 3^{rd},..., n^{th} resonance frequencies and to suppress them. Note that, whenever a new resonance is detected, a multi-tuned damping control (as per (7)) should be implemented to cover all the early detected resonance frequencies. This process involves the simultaneous design of multiple narrowband damping control loops, each corresponding to one of the detected resonance frequencies. Without this procedure, and by simply adding a single-tuned damper at the newly detected resonance frequency, the mutual coupling effect can potentially degrade the performance of the dampers that were applied at the resonance frequencies detected earlier. In contrast to the existing approach in [5] where multiple resonances are detected and damped all at once, the proposed approach focuses on one resonance at a time, which allows us to target resonances as they emerge and applying a simpler design. It also reduces the risk of false positives, i.e., detecting a resonance due to cross-spectral interference.

B. Parameterization and Adaption of Damping Gain

1) Initialization of x_k and K_{dk}

Based on the discussion in Section III-B, the damping gain K_{dk} is determined by an initial selection of x_k for the CCF programmed at f_{rk}, which can be either 1 if $\mathfrak{Re}\{Y_p(j\omega_{rk})\} > 0$, or 2 if $\mathfrak{Re}\{Y_p(j\omega_{rk})\} < 0$. This initial selection of x_k defines the minimum required damping gain for CCF at f_{rk}, which is generally enough to guarantee the resonance at f_{rk} can be damped after applying the damping control. On the other hand, even if such selection cannot provide sufficient damping at f_{rk} in certain scenario, this initial value of x_k gives a "nominal" positive conductance at f_{rk}. Any further adjustment on x_k represents a "perturbation" around its initial point. With such initial selection of x_k mentioned above, the detected resonances can be effectively damped when the MMC is connected to a passive grid. This is due to the fact that the net-damping is guaranteed to be greater than 0 as long as the negative damping of MMC is compensated, considering that inherent resistance always exists in the passive grid. However, in the condition that the MMC is connected to an active network that includes power converters, x_k may need to be adjusted to a higher value to provide additional damping around the resonance frequency.

2) Adjustment on x_k and K_{dk}

Assuming that the frequency of a resonance is f_{rk}, the initialization of x_k discussed above ensures no drift of resonance frequency after applying the CCF-based damping control at f_{rk}, even when the added damping is insufficient to mitigate the system resonance. After applying the damping controllers, if the detected resonance remains at f_{rk}, it obviously indicates that K_{dk} calculated using x_k does not provide sufficient positive damping at f_{rk} to ensure a positive net-damping. Then, x_k can be increased to a higher value in a fixed step (e.g., 0.1 pu), in order to further enlarge the added amount of damping at f_{rk}. It is duly noted that by further increasing x_k and consequently on K_{dk}, the virtual conductance introduced by the damping control could cause a slight magnitude change of $Y_{pd}(s)$ around f_{rk}. As a result, the magnitude intersection frequency (i.e., resonance frequency) may shift. In such a case, the online resonance detection might identify a "new" resonance located inside (f_{uk}, f_{lk}) (see (12)) around f_{rk}. Once the amplitude of the resonance component around f_{rk} is brought down to a value smaller than the threshold, x_k can be maintained at its current selection.

Note that the aforementioned procedure of adjustment on x_k is equivalent to amplifying x_k by a nonlinear gain defined as

$$f(h,w,a,x_k) = h\left[\frac{\tanh(\frac{ax_k}{w} - a\lfloor\frac{x_k}{w}\rfloor - \frac{a}{2})}{2\tanh(\frac{a}{2})} + \frac{1}{2} + \lfloor\frac{x_k}{w}\rfloor\right] \quad (11)$$

where h is the height of the fixed step (e.g., 0.1), w represents one sampling time step T_s, a determines the smoothness of the step increasing, which is usually selected as 200.

C. Parameterization and Adaption of the Width of Damping Band

1) Definition of the Width of Damping Band

The term damping band f_{dbk} for the damping control programmed at f_{rk} is defined to be the frequency range around f_{rk} where the phase response of $Y_{rk}(s)$ is inside [-90°, 90°]. Based on (2) and (3), given the ω_{bk} and ω_r of $H_{ccf}(s)$, the width of the damping band f_{dbk} can be obtained by numerically evaluating the following expressions.

$$\begin{cases} \omega_{lk} = \mathbf{max}\{\mathsf{FindRoot}[\frac{e^{j\omega_{rk}T_d}e^{-j\omega T_d}H_{ccf}(j\omega)}{N_p(j\omega)} = 0, x \le \omega_{rk}]\} \\ \omega_{uk} = \mathbf{min}\{\mathsf{FindRoot}[\frac{e^{j\omega_{rk}T_d}e^{-j\omega T_d}H_{ccf}(j\omega)}{N_p(j\omega)} = 0, x \ge \omega_{rk}]\} \\ f_{dbk} = \omega_{uk}/(2\pi) - \omega_{lk}/(2\pi) = f_{uk} - f_{lk} \end{cases} \quad (12)$$

where, FindRoot denotes a function returns the roots of the polynomial represented by $e^{j\omega_{rk}T_d}e^{-j\omega T_d}H_{ccf}(j\omega)/N_p(j\omega)$, which can be programmed in any available numerical computing environment.

2) Fixed Selection of ω_{bk} for a Proper f_{dbk} around f_{rk}

To adaptively mitigate the detected resonance at f_{rk} by applying the CCF-based damping control, one issue is how to choose the value of ω_{bk} of CCF for the purpose of defining a proper width of the damping band, so that the resonance is effectively mitigated without introducing unwanted consequences at other frequencies. As a general rule, the passivity of MMC is improved over a wider range of f_{rk} with an enlargement of ω_{bk}. However, setting a large ω_b may conflict with the purpose of narrowband damping. In light of the authors' experience with the impedance characteristics of MMCs and various passive grids in practical projects, it is recommended to generally select ω_{bk} within the range of $2\pi\cdot 40 \sim 2\pi\cdot 80$ rad/s for the CCF at f_{rk}.

3) Adaptive Tuning on ω_{bk} for an Optimal f_{dbk} around f_{rk}

However, there are still has to be a mechanism to adaptively regulate the selection of ω_b in two scenarios:

- The resonance f_{rk} occurs in a frequency range close to 2^{nd}-order harmonic frequency and a fixed selection on ω_{bk} may deteriorate the main control functions of MMC
- Multiple resonances occur close to each other, a fixed selection of ω_{bk} for all the CCFs may cause CCFs' damping bands overlap considerably with each other. This would result in each damper introducing a certain amount of virtual admittance to others, which may move the detected resonances to the frequency range without sufficient positive net-damping.

Based on these considerations, a method to adaptively regulate the ω_{bk} of CCF at f_{rk} according to the system resonance condition at f_{rk} is shown in Fig. 2. After the resonance at f_{rk} is detected, its amplitude $A(f_{rk})$ is continuously compared with the threshold value A_{th} each sampling time step. The error is then fed into a PI compensator, and the output of PI compensator is summed with an initial value $\omega_{b0}=2\pi\cdot 5$ rad/s to obtain the reference command of CCF's bandwidth (marked as ω^*_{bk}). This allows the bandwidth of the CCF at f_{rk} to be dynamically adjusted to maintain a minimum required ω_{bk} at f_{rk}.

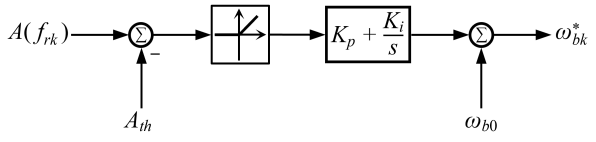

Fig. 2. Adaptive regulation strategy for ω_{bk}.

D. Algorithm for Adding and Adjusting Damping Controls

The pseudocode for adding and adjusting damping controls is reported in **Algorithm 2**, which also displays the processes necessary for implementing the parameterization and adaptation strategies as discussed in Sections V-B and V-C. $\overrightarrow{F_r}$ represents all the early detected resonance frequencies; Matrices $\mathbb{Y}^{-1}$, $\mathbb{X}$ and $\boldsymbol{b}$ in the input of **Algorithm 2** are calculated based on (8). It should be noted that, the penultimate detected resonance frequency in $\overrightarrow{F_r}$ is denoted as $f_r^{'}$, which is different from the newly detected resonance at f_{rk}.

Algorithm 2 Adding and Adjusting Damping Controls

Input: $\overrightarrow{F_r}=(f_{r1},f_{r2},...,f_{rn})$, $f_r^{'}$, $\mathbb{Y}^{-1}$, $\mathbb{X}$, $\boldsymbol{b}$, f_{rk}
Output: 1) $\overrightarrow{K_d}=(K_{d1},K_{d2},...,K_{d(n-1)},K_{dn},K_{dk})$; 2) $\overrightarrow{\theta_d}=(\theta_{d1},\theta_{d2},...,\theta_{d(n-1)},\theta_{dn},\theta_{dk})$;

1: **for** $j=1,2,3,\ldots,$**sizeof**$(\overrightarrow{F_r})$ **do**
2: Calculate f_{uj} and f_{lj} based on (12)
3: **if** $f_{rk}\in[f_{lj},f_{uj}]$ **then**
4: **if** $f_{rk}=f_r^{'}$ **then**
5: $x_j=x_j+0.1$; Update $\overrightarrow{K_d}$; **BREAK**
6: **else**
7: **if** "$\Re\mathfrak{e}\{Z_p(j2\pi f_{rk})\}<0$ & $x_j>2$" or "$\Re\mathfrak{e}\{Z_p(j2\pi f_{rk})\}\geq 0$ & $x_j>1$" **then**
8: $x_j=x_j+0.1$; Update $\overrightarrow{K_d}$; **BREAK**
9: **else**
10: Calculate f_{uk} and f_{lk}
11: **if** $f_{uk}\in[f_{lj},f_{uj}]\mid f_{lk}\in[f_{lj},f_{uj}]$ **then**
12: Activate adaptive tuning of ω_{bk} and ω_{bj}
13: Obtaining ω^*_{bk} and ω^*_{bj}
14: Update $\overrightarrow{K_d}$; Update $\overrightarrow{\theta_d}$ **BREAK**
15: **else**
16: **if** $\Re\mathfrak{e}\{Z_p(j2\pi f_{rk})\}\geq 0$ **then**
17: $x_k=1$;
18: **else**
19: $x_k=2$;
20: Include x_k into $\mathbb{X}$; Include $\mathbf{Y}_{dk}(j\omega_{rk})$ into $\mathbb{Y}^{-1}$; Include $\Re\mathfrak{e}\{Z_p(j2\pi f_{rk})\}$ into $\boldsymbol{b}$
21: Update $\overrightarrow{K_d}$; Update $\overrightarrow{\theta_d}$

Algorithm 3 Remove Redundant Damping Controls

Input: $\overrightarrow{F_r}=(f_{r1},f_{r2},...,f_{rn},f_{rk})$;
Output: 1) $\overrightarrow{F_{ru}}$; 2) f_{rs}

1: $\overrightarrow{F_{ru}}=(f_{r1},f_{r2},...,f_{rs},...,f_{r(n-1)},f_{rn},\cancel{f_{rk}})$;
2: **for** $s=1,2,3,\ldots,$**sizeof**$(\overrightarrow{F_r})$ **do**
3: Take the frequency f_{rs} at which the MMC has the lowest negative damping among all the $\Re\mathfrak{e}\left[Z_p(j2\pi f_r)\right]$, $f_r\in\overrightarrow{F_r}$
4: $\overrightarrow{F_{ru}}=(f_{r1},f_{r2},\ldots,\cancel{f_{rs}},\ldots,f_{r(n-1)},f_{rn})$
5: $\overrightarrow{F_r}=(f_{r1},f_{r2},\ldots,\cancel{f_{rs}},\ldots,f_{r(n-1)},f_{rn})$
6: Program MCCF based on $\overrightarrow{F_{ru}}$
7: **if** newly detected resonance frequency $f_{new}<f_{rs}\pm\omega_b/(2\pi)$ **then**
8: Include f_{rs} in $\overrightarrow{F_{ru}}$; Program MCCF based on $\overrightarrow{F_{ru}}$; Repeat from line 2
9: **else**
10: Repeat from line 2

E. Remove Redundant Damping Controls

In a practical system, a detected resonance, for instance at f_{rk}, could disappear due to the change in system operating conditions and network configurations. In this subsection, we propose the **Algorithm 3**, capable of automatically disabling previously employed damping controllers one by one. However, if a resonance is still present, the algorithm would automatically turn on the corresponding damping control again.

The method starts in line 1, with the assignment of all previously detected resonance frequencies to $\overrightarrow{F_{ru}}$. A sorting process is then performed to determine the resonance frequency f_{rs}

at which the MMC has the smallest negative damping (line $2 \sim 3$). Since the algorithm assumes that the new resonance is a result of change of system resonance conditions, and some previously detected resonance may already have disappeared, it disables the damping controller centering at f_{rs} first (line $4 \sim 5$). In addition, MCCF based multi-tuned damping will be re-programmed and only tackle to the remaining resonance frequencies (line 6). The design of MCCF-based multituned damping will take the resonance at f_{rs} into account again if a new resonance around f_{rs} reappears (line $7 \sim 8$). Otherwise, it indicates that damping control is not required around f_{rs}. Multiple iterations of the above procedures may be performed until all the disappeared resonances are identified and the corresponding damping controls are turned off (line $9 \sim 10$).

VI. Case Study and Simulation Validation

To validate the performance of the proposed adaptive damping control in mitigating resonances of MMC-based applications, three examples based on detailed EMT simulations are presented in this section. Each of the examples demonstrates a practical issue that is either difficult to address using existing methods, or currently lacks a viable solution. The electrical parameters of MMC's power stage and the ac systems are tabulated in Table I, while the control design of MMC are provided in Table II.

TABLE I
Electrical Parameters of MMC and AC Systems

Parameter	Symbol	Value	Unit
Rated active power	P_N	900	MW
Rated ac side voltage	U_N	300	kV rms ph-ph
Rated dc side voltage	V_{dc}	± 320	kV
Arm impedance	$R_s + jL_s$	$0.1 + j0.05$	Ω
Submodules per arm	N_{sm}	50	-
Submodule capacitance	C_{sm}	1.2	mF
Time delay	e^{-sT_d}	200	μs
OTL series impedance	$R_0 + jL_0$	$(29.8 + j1.58) \times 10^{-3}$	Ω /mile
OTL shunt impedance	jC_0	$j17.9 \times 10^{-9}$	F/mile
Cable series Impedance	$R_c + jL_c$	$(30 + j0.35) \times 10^{-3}$	Ω /mile
Cable shunt Impedance	jC_c	$j340 \times 10^{-9}$	F/mile

TABLE II
Control Specifications for MMC

Control functions	K_p	K_i	K_d
DC voltage control	0.0065	0.2	NA
AC current control (case I)	22.2	27915.5	7.85
AC current control (case II)	27.2	19739.2	7.85
Circulating current control	22.2	13957.7	31.42
Phase-locked loop	1.48×10^{-4}	0.0093	N/A
AC voltage control (case III)	0.5	54.4	N/A

A. Damping HFR between GFL-MMC and Long Overhead Lines

1) Case Description and Simulation Setup

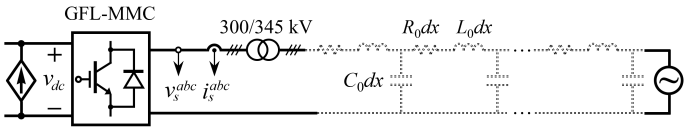

Fig. 3. An GFL-MMC-based grid integration via long overhead transmission.

The grid-following (GFL) MMC-based integration of renewable energy (RE) has been known to suffer from multiple HF resonances issue when MMC is imposed to long overhead transmission lines (OTL) or HVac cables [2], [5]. Long overhead transmission lines (OTL) or cables exhibit multiple parallel and series resonances due to their distributed nature, specifically, the inductive and capacitive components along the entire length of the line. In addition, the resistance per unit length of the transmission line is typically small, causing the phase response of OTL to changes between values nearing $\pm$ 90°. As a result, the multiple high-frequency (HF) resonances between the MMC and the OTL/cable are either unstable or poorly damped.

As noted in [2], [5], when a single-tuned damper is added to mitigate an inherent single resonance between MMC and OTL, an original poorly-damped resonance at the neighboring frequencies of the added damper might become negatively damped, developing a new unstable HFR. The first example is specifically designed to validate the proposed adaptive damping control in such a scenario, which involves a GFL-MMC integrated to a grid by a 345 kV 100-mile OTL. The equivalent circuit is depicted in Fig. 3 and electrical parameters are tabulated in Table I. Note, to accurately represent the high-frequency characteristics of OTL, the frequency-dependent model [18] is employed for OTL modeling. The GFL-MMC is operated in dc voltage control mode with unity power factor, and the control parameters are specified in Table II, while the configuration of online resonance detection is shown in Table III.

TABLE III
Configuration of Online Resonance Detection in Case I

Parameter	Symbol	Value
Sampling frequency	f_s	100 kHz
Window size of STFT	N	2000
Hop-size of STFT	N_{hop}	1000
Analyzed # of windows (Algorithm 2)	q	3
Detection Threshold (Algorithm 2)	A_{th}	$5\% \ \frac{\sqrt{2}}{\sqrt{3}} \frac{P_N}{U_N}$
Bandwidth of CCFs	ω_{bk}	80 Hz

2) Simulation Verification

Fig. 4 shows the simulated responses of this system. As can be seen from Fig. 4, when GFL-MMC starts to connect to the OTL, an electrical transient is initiated at 716 Hz and it dominates the short-time spectrum within two consecutive time recording segments. This transient is correctly identified by **Algorithm 1**, thereby no active damping control reacts to it. An unstable 1551 Hz resonance is measured at t = 0.072

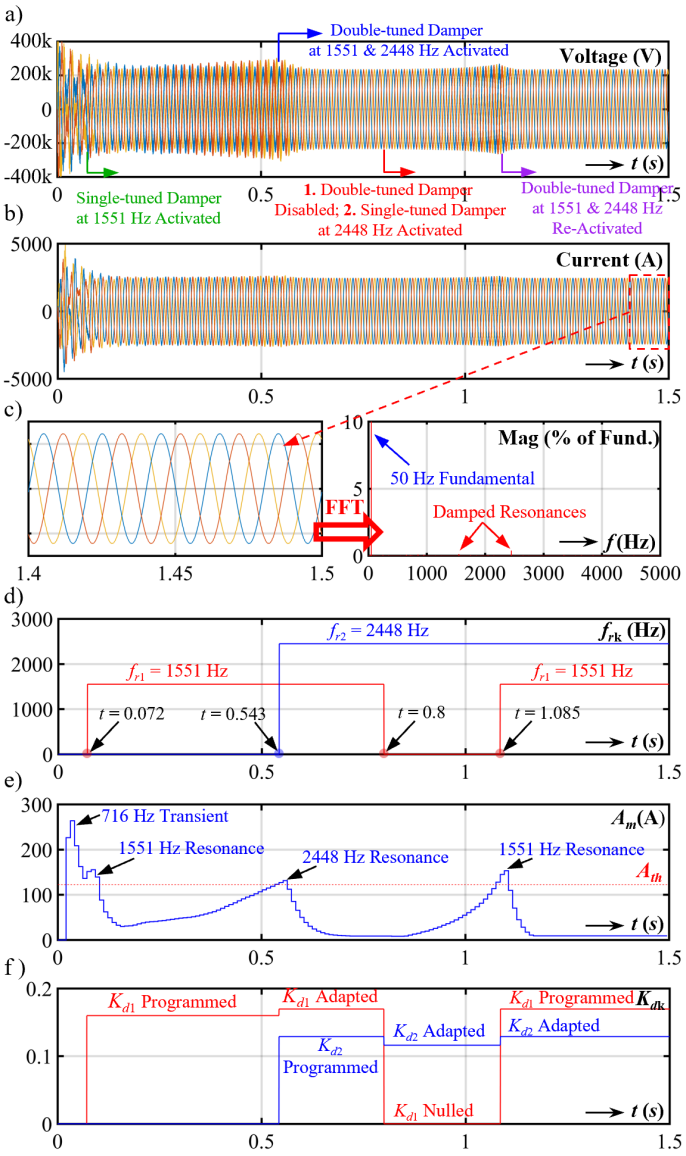

Fig. 4. Simulated time-domain responses of: a) MMC voltage and b) MMC current; c) zoom-in view and FFT analysis of MMC current between 1.4 $s \sim$ 1.5s. Online resonance detection outputs: d) detected resonance frequency f_r; e) spectral peak on the STFT spectrum; f) programmed and updated damping gains of CCFs

s, where a single-tuned damping control is conducted, which adds positive damping around 1551 Hz. The parameters of the single-tuned damping control are automatically calculated as: f_{r1} = 1551 Hz, K_{d1} = 0.1599, θ_1 = -153.90°. Following this event, **Algorithm 1** identifies that the system exhibits another unstable resonance at 2448 Hz at t = 0.543 s. As a result, **Algorithm 2** programs a double-tuned damper to simultaneously provide positive damping around both 1551 Hz and 2448 Hz. Based on (7), the parameters of the double-tuned damping control are given by: f_{r1} = 1551 Hz, K_{d1} = 0.1696, θ_1 = -153.90°; f_{r2} = 2448 Hz, K_{d2} = 0.129, θ_2 = -90.76°.

At t = 0.8 s, to examine whether the damper at 1551 Hz should be retained or not, **Algorithm 3** deactivates the damper at 1551 Hz (i.e., set $K_{d1} = 0$), and adpates the double-tuned damper to a single-tuned damper centered solely at 2448 Hz, as indicated by the falling edge of red solid line in Fig. 4 d) at t = 0.8 s. It should be noted that the damping gain of the single-tuned damper at 2448 Hz also needs to be updated to maintain the added positive resistance at 2448 Hz as it is when a double-tuned damper is used. Otherwise, an over-compensation for the negative damping at 2448 Hz might occur, causing the resonance frequency to drift from 2448 Hz into a region lacking sufficient positive damping. The parameters of single-tuned damping are updated to: f_{r2} = 2448 Hz, K_{d2} = 0.1162, θ_2 = -90.76°. From Fig. 4 a), b) and e), it can be seen that the 1551 Hz resonance starts again after the damper at 1551 Hz is disabled, indicating that the resonance condition still exists and the damping control is still required at 1551 Hz. This 1551 Hz resonance is re-detected by **Algorithm 1** at t = 1.085 s, and the double-tuned damping control is automatically reactivated at the same time, thereby the detected 1551 Hz resonance is suppressed. The FFT analysis of MMC current between 1.4 s to 1.5 s shows that the system contains virtually no oscillations at 1551 Hz and 2448 Hz, which validates the effectiveness of the proposed adaptive damping control.

3) Comparison with Existing Method

The proposed adaptive damping scheme is compared with two other adaptive damping methods mentioned in introduction: the adaptive impedance compensation method [7] (marked as *Method 1*) and adaptive notch filter method [8] (marked as *Method 2*).

In addition, the amplitude threshold used in both *Method 1* is chosen to be $5\%I_g$, where I_g is the peak value of fundamental current. The amplitude threshold and frequency threshold in *Method 2* is set to 2% I_g and 200 Hz, as discussed in [8]. As shown in Fig. 4 e), the 716 Hz resonance initially persists as the spectral peak and its amplitude remains above A_{th} within the first few FFT windows. This observation clearly highlights the inability of *Method 1* and *Method 2* to differentiate between 716 Hz electrical transients and unstable system resonance. Therefore, to ensure a fair comparison, online resonance detection in *Method 1* and *Method 2* will be conducted after the transient disappears to avoid false detection.

The 2^{nd}-order bandpass filter-based damping function in *Method 1* is designed to have the same cutoff frequency as the one described in this work, and the damping gain is adjusted to provide an equivalent amount of positive damping at the detected resonance frequency. The notch filter in *Method 2* is tuned according to Eq. (12) in [8]. The simulated current responses of the MMC equipped with *Method 1* and *Method 2* are depicted in Fig. 5. As observed in Fig. 5 a) and b), *Method 1* mitigates the unstable resonance at 1551 Hz, but fails to mitigate the other unstable resonance at 2448 Hz, as it cannot resolve multiple resonances. On the contrary, Fig. 5 c) and d) shows that *Method 2* suppresses the 1551 Hz unstable resonance without exciting a 2448 Hz unstable resonance. However, a stable resonance with a magnitude of $2.6\%I_g$ at 2448 Hz sustains in the system, as indicated by the small ride-on inter-harmonic in the simulated current response and the corresponding Fourier analysis displayed in Fig. 5

d). This lingering inter-harmonic is attributed to the poorly damped impedance response of the MMC at 2448 Hz, which will be discussed subsequently. The threshold-based detection in *Method 2* identifies the sustained resonance at 2448 Hz as a new resonance at approximately 0.5 s and promptly adapts the center frequency of the notch filter accordingly. However, as the unstable resonance condition at 1551 Hz persists, this adaptation leads to the re-emergence of unstable oscillation events at 1551 Hz. This behavior is represented in the two subfigures on the right-hand side of Fig.5 d).

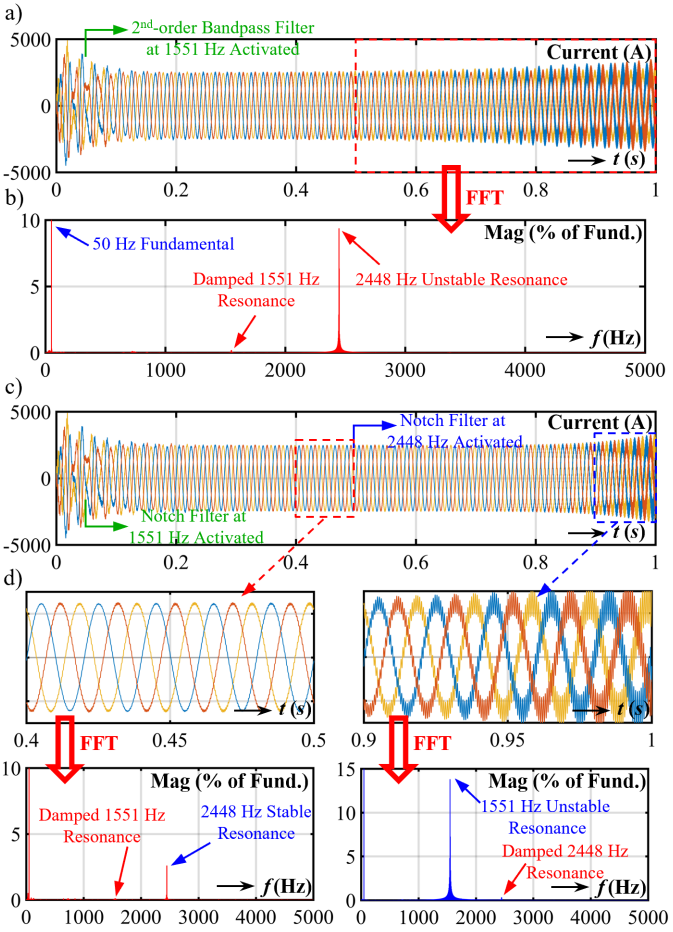

Fig. 5. a) simulated current of MMC with *Method 1*; b) Fourier analysis of current in a) within 0.5 $s \sim 1$ s; c) simulated current of MMC with *Method 2*; d) Fourier analysis of current in c) within 0.4 $s \sim 0.5$ s and 0.9 $s \sim 1$ s

4) Further Validation via Impedance Responses

The impacts of the three aforementioned methods on the overall MMC impedance are plotted against each other along with the grid impedance (denoted as Z_g) in Fig. 6. The subscript "pd_pro", "pd_M1", and "pd_M2" represent the MMC impedance damped by the proposed damping method, *Method 1*, and *Method 2*, respectively. The phase differences between $Z_p(s)$ and $Z_g(s)$, $Z_{pd\_pro}(s)$ and $Z_g(s)$, $Z_{pd\_M1}(s)$ and $Z_g(s)$, and $Z_{pd\_M2}(s)$ and $Z_g(s)$ are listed in Table IV. As indicated by this table, the MMC and OTL inherently contain an unstable resonance at 1551 Hz and a lightly damped resonance at 2448 Hz. *Method 1* reduces the phase difference between MMC and OTL to 172.84°, but increases the phase difference at 2448 Hz

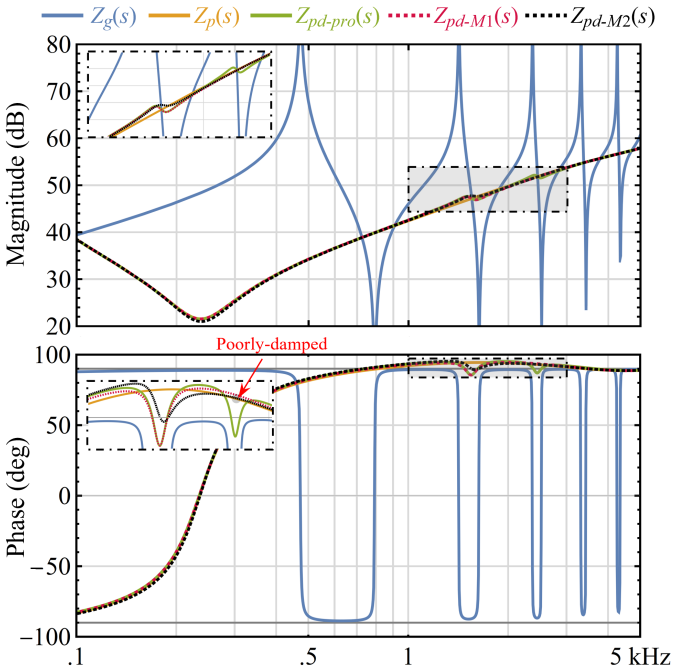

Fig. 6. Impedance responses of: undamped GFL-MMC (solid orange), damped MMC with proposed damping control (solid green), damped MMC with *Method 1* (dashed red), damped MMC with *Method 2* (dashed black) against OTL impedance (solid blue)

to 180.4°. This induces an unstable resonance at 2448 Hz, as depicted in Fig. 5 a) and b). Even though *Method 2* has less impact on the phase response of MMC at 2448 Hz compared to *Method 1*, it brings the phase difference between MMC and the OTL more closer to 180°, indicating the emergence of a sustained oscillation with a large amplitude at 2448 Hz. Given that the amplitude of 2448 Hz components exceeds the $2\%I_g$ threshold, it triggers textitMethod 2 to adjust the notch filter to 2448 Hz, making 1551 Hz resonance grow again. On the contrary, the proposed adaptive damping control demonstrates its damping effect at both 1551 Hz and 2448 Hz. This is supported by Table IV, where the phase differences between MMC and OTL at 1551 Hz and 2448 Hz are reduced to 172.82° and 173.81°, respectively.

TABLE IV
PHASE DIFFERENCE BETWEEN MMC AND AC SYSTEM AT INTERSECTION FREQUENCIES

	1551 Hz	2448 Hz
$\angle Z_p(s) - \angle Z_g(s)$	181.65°	179.81°
$\angle Z_{pd\_pro}(s) - \angle Z_g(s)$	172.82°	173.81°
$\angle Z_{pd\_M1}(s) - \angle Z_g(s)$	172.84°	180.40°
$\angle Z_{pd\_M2}(s) - \angle Z_g(s)$	177.42°	179.92°

B. Damping HFR Changed with Grid Variation

1) Case Description and Simulation Validation

The aim of this subsection is to test the robustness of the proposed adaptive damping control against grid variation. The example also represents a practical reason for HFR in a GFL-MMC-based system [4], which is also noted as a consecutive HFR events in [8]. The schematic of the simulation model is

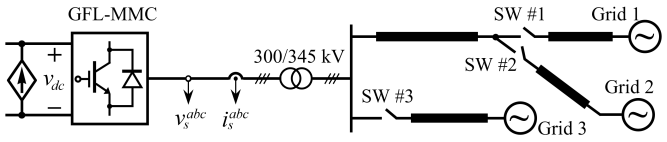

Fig. 7. An GFL-MMC integrated into a radial transmission system

depicted in Fig. 7. The configuration of the online resonance detection is the same to what is used in case 1, which has been displayed in Table III.

The simulation starts with Switch #1 closed, while Switches #2 and #3 are initially open. At $t = 0.2$ s, Grid 2 is incorporated into the power system by closing Switch #2. At $t = 0.5$ s, Grid 2 is disconnected from the system and Grid 3 is integrated into the power system. The simulated GFL-MMC current response and the data processed by online resonance detection are illustrated in Fig. 8. The first resonance at 2289 Hz, detected by **Algorithm 1** at $t = 0.246$ s after the connection of Grid 2, and **Algorithm 2** triggers the initiation of a single-tuned damping control at 2289 Hz. Parameters for the single-tuned damping control are automatically calculated as: f_{r1} = 2289 Hz, K_{d1} = 0.1321, θ_1 = -101.7°. Upon disconnection of Grid 2 from the system and subsequent connection of Grid 3, the second resonance is measured to be 2603 Hz at t = 0.553 s. A double-tuned damping control is correspondingly designed to add positive damping to MMC around both 2289 and 2603 Hz, which promptly mitigates the resonance at the 2603 Hz frequency with the damper at 2289 Hz sustained.

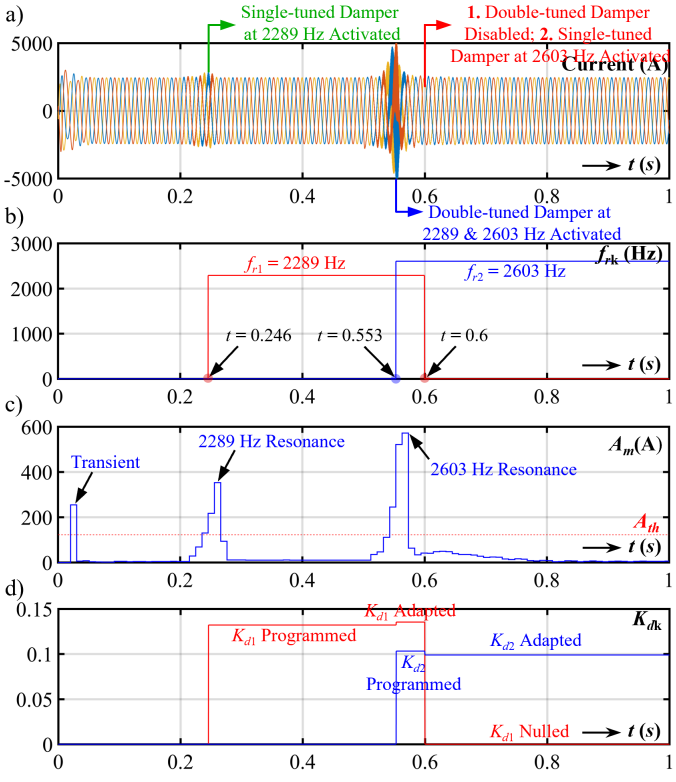

Fig. 8. a) Simulated time-domain responses of MMC current. Online resonance detection outputs: b) detected resonance frequency f_r; c) spectral peak on the STFT spectrum; d) programmed damping gain of CCFs

The parameters for the double-tuned damping control are as follows: f_{r1} = 2289 Hz, K_{d1} = 0.135, θ_1 = -101.7°; f_{r2} = 2603 Hz, K_{d2} = 0.103, θ_2 = -80.04°. To determine whether the new resonance is a consequence of the variation of the grid configuration, **Algorithm 3** disables the damping control at 2289 Hz (i.e., K_{d1} = 0) at $t = 0.6$ s, adjusting the double-tuned damping control to a single-tuned damping centered at only 2603 Hz. The single-tuned damping parameters are then updated to: f_{r2} = 2603 Hz, K_{d2} = 0.0989, θ_2 = -80.04°. As evident from Fig. 8, without damping control at 2289 Hz, the system still maintains a stable operation, indicating the disappearance of the 2289 Hz resonance. Thus, the proposed online detection algorithm successfully identifies the changes of resonance condition due to the grid variations, while the adaptive control correspondingly eliminates redundant damping controls, demonstrating high robustness of the proposed adaptive control to grid variation.

2) Comparison with Existing Method

For comparison, *Method 2* is also simulated under the same conditions, while *Method 1* is excluded due to its inability to monitor and mitigate consecutive high-frequency (HF) resonances. The setup for *Method 2* remains identical to that used in Case I, with the amplitude threshold changed to $5\%I_g$ to facilitate a fair comparison. The simulated current response and the resonance detection result are shown in Fig. 9. As shown in Fig. 9, the 2289 Hz resonance is detected at $t = 0.226$ s, the adaptive notch filter is tuned to 2289 Hz immediately, and the unstable 2289 Hz resonance is subsequently mitigated. Upon disconnecting Grid 2 and involving Grid 3, the frequency component at 2603 Hz exceeds the threshold value of $5\%I_g$ at ~ 0.5 s. As a result, the adaptive notch filter is re-tuned to 2603 Hz, and the 2603 Hz resonance is suppressed. As evident from Fig. 8 and Fig. 9, *Method 2* detects each resonance one fundamental cycle faster than the proposed method. This difference in resonance detection speed is due to the different resonance identification algorithm utilized by **Algorithm 2** and *Method 2*. Specifically, **Algorithm 2** adopts a ROC-based detection approach, necessitating data from a minimum of three sequential Fourier analysis windows to determine the presence of a resonance. On the contrary, *Method 2*

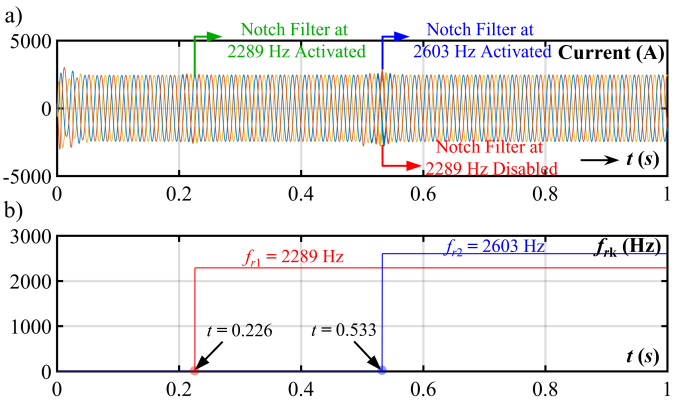

Fig. 9. a) Simulated time-domain current responses of MMC equipped with *Method 2*; b) detected resonance frequency f_r.

classifies a frequency component as an unstable resonance as soon as its amplitude exceeds a predefined threshold value. However, it should be noted that, the ROC-based resonance identification in **Algorithm 2** ensures more accurate and reliable resonance detection compared to the simple threshold value-based method used in *Method 2*.

C. Damping Resonance Involving Grid Forming MMC and Wind Farm

1) Case Description and Simulation Validation

The aim of the third case study is to validate the efficacy of the proposed adaptive damping controls in suppressing two characteristic resonances that typically occur during the integration of a wind farm into grid forming (GF) MMC. These resonances are develped under two scenarios as follows:

- Prior to the connection of turbines to the wind farm collection network, an GF-MMC needs to energize the network. During this process, the negatively damped MMC may form a resonance with the capacitive impedance of the wind farm cable network.
- The control delay of the turbine converter and the low pulse width modulation (PWM) frequency can introduce negative damping around the parallel resonance (e.g., the parallel resonance formed by the *LCL* filter of the turbine converter) of the wind farm impedance. A resonance can occur between the MMC and the entire wind farm, including the collection network and turbine converters, in the frequency range immediately following the parallel resonance of the wind farm impedance.

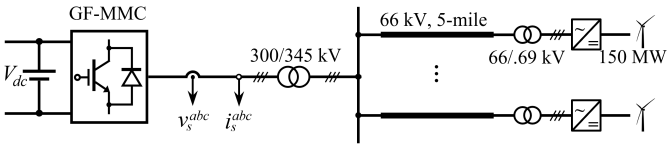

Fig. 10. An GF-MMC-based offshore wind integration via cable network

Fig. 10 shows the system under study, there are six 5-mile cable strings rated at 66 kV, and the terminal of each string is connected by an aggregated 150 MW Type-IV turbine interfaced via a 0.69/66 kV step-up transformer. The six strings are collected and the voltage is stepped up to 300 kV to interconnect with the MMC. A 2.5 kHz double-edged sampling-based PWM and 200 μs digital control delay are included in the design of Type-IV turbine model. After the wind farm collection network is energized, all six turbines are programmed to connect simultaneously at full power to simplify the simulation process. In this example, the MMC operates with online resonance detection based on MMC voltage measurement. The setup of online resonance detection unit includes the following parameters: sampling frequency f_s = 100 kHz; N = 2000, N_{hop} = 1000; q = 3; A_{th} = 8%V_g, where V_g represents the amplitude of the rated MMC voltage at the fundamental frequency. It should be noted that the resonance between the MMC and the cables can begin to emerge at lower frequencies (around $\sim$ 300 Hz), as the cables possess a higher shunt capacitance compared to the overhead transmission lines. In this case, ω_b is initially set at 40 Hz for the CCF centered at first detected resonance.

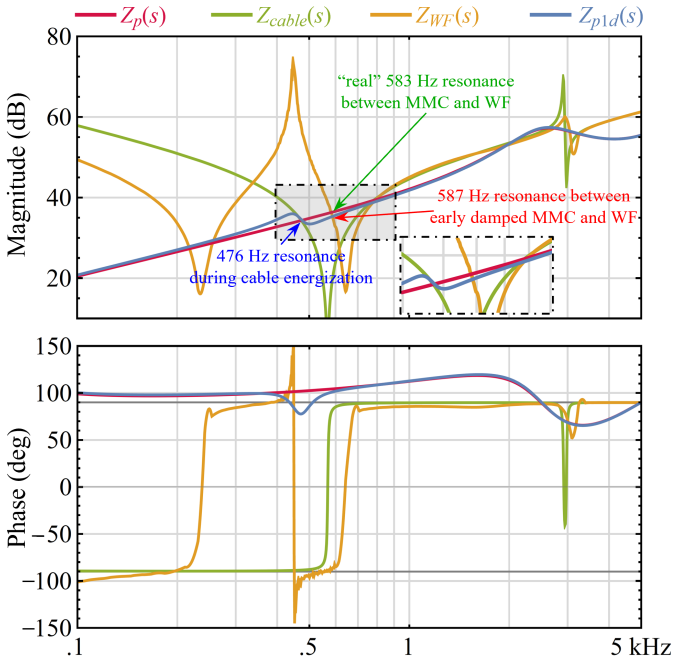

Fig. 11. Impedance responses of: undamped GF-MMC (red), damped MMC with single-tuned damper at 476 Hz (blue), entire wind farm impedance including wind turbines (orange) against cable impedance (green)

2) Impedance-based Analysis and Simulation Verification

Fig. 11 illustrates the impedance responses of the undamped GF-MMC (marked by $Z_p(s)$), the wind farm collection network composed of cables (denoted as $Z_{Cables}(s)$), and the impedance of entire wind farm comprising turbine converters operating in full-power mode (marked as $Z_{WF}(s)$). The impedance of GF-MMC intersects with the impedance of cable network at multiple points. However, only the point at 476 Hz exhibits a negative net-damping, which is $\Re\mathfrak{e}\,[Z_p(j2\pi476)+Z_{Cable}(j2\pi476)]$ = -9.37Ω. This indicates the occurrence of an unstable resonance at 476 Hz when the GF-MMC begins energizing the cable network before turbines are integrated. With the proposed adaptive damping method, resonances should be automatically detected first and subsequently suppressed by a single-tuned damping control added at 476 Hz. This results in a damped MMC impedance, denoted as $Z_{p1d}(s)$, as plotted by the blue line in Fig.11. After this single0-tuned damping control is conducted, the net-damping at 476 Hz increases to 12.63 Ω, allowing the turbines to be stably connected to the cable network. Nevertheless, as indicated in Fig.11, the full-power wind farm impedance $Z_{WF}(s)$ intersects with the damped MMC $Z_{p1d}(s)$ at 587 Hz, at which point the net-damping between $Z_{WF}(s)$ and $Z_{p1d}(s)$ equals -22.21 Ω. Therefore, the proposed adaptive damping control is expected to accomplish the following four objectives:

- The adaptive damping control should automatically detect the 587 Hz resonance and then configure a double-tuned damper to add positive damping simultaneously at 476 Hz and 587 Hz.

- The damping control centered at 587 Hz should be equipped with an adaptive methodology to select the bandwidth of CCF centered at this frequency. This is due to the close proximity of 587 Hz resonance to the resonance at 476 Hz. An inappropriate selection of the CCF's bandwidth at 587 Hz could induce unwanted interference with the damper at 476 Hz.
- Given that the wind farm impedance does not intersect with the MMC at 476 Hz (see Fig. 11), the adaptive damping control should have the ability to disable the damping control at 476 Hz.
- Following the release of the damping control at 476 Hz, the adaptive damping control should be able to detect the "real" unstable resonance at 583 Hz and adapt the damping control to suppress it accordingly.

To validate the predictions of the aforementioned impedance-based analysis and to assess the expected performance of the proposed adaptive damping control, an EMT simulation of the system is executed. Fig. 12 illustrates the voltage response of MMC, along with the output of the online resonance detection and adaptive algorithms.

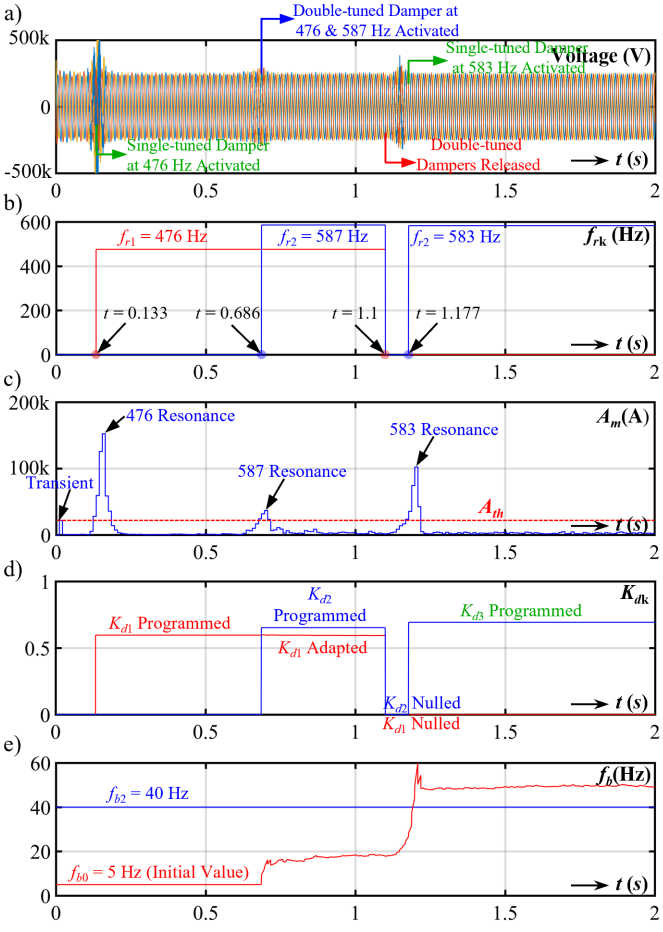

Fig. 12. a) Simulated time-domain responses of GF-MMC voltage. Online resonance detection output: b) detected resonance frequency f_r; c) the spectral peak in STFT spectrum; d) damping gains of CCFs; e) bandwidth of the CCFs for: the damper at 476 Hz (blue), and the damper at 583 and 587 Hz (red)

The energizing of the wind farm cables begins at t = 0.1 s, during which the 476 Hz resonance drives an unstable voltage oscillation. **Algorithm 1** identifies the 476 Hz resonance at t = 0.133 s and applies a single-tuned damper with a fixed 40 Hz CCF at 476 Hz, immediately eliminating the resonance and henceforth allows the start-up of wind turbines to start at t = 0.6 s. The ac network impedance then changes from $Z_{cable}(s)$ to $Z_{WF}(s)$, creating another unstable resonance with $Z_{p1d}(s)$ at 587 Hz, which is detected at t = 0.686 s. The adaptive damping control initially treats the system containing two resonances and employs a double-tuned damper targeting 476 and 587 Hz simultaneously. Due to the proximity of 587 Hz and 476 Hz, the damper at 587 Hz utilizes a CCF with an adaptive bandwidth regulated by a PI compensator, as described in Fig.2. As evident from the red line in Fig.12 e), the adaptively regulated bandwidth for the CCF at 587 Hz is approximately 19 Hz when the double-tuned damper is activated. At t = 1.1 s, **Algorithm 3** automatically deactivates the double-tuned damper to find out the frequencies where resonances no longer exist. This causes an unstable resonance at 583 Hz to immediately emerge, as predicted by the impedance analysis in Fig.11. To mitigate the resonance, a single-tuned damper is then applied at 583 Hz, suppressing the resonance within half a fundamental cycle, as indicated by the decreased spectral peak in Fig.12 c).

VII. Conclusion and Future Work

This paper introduces an adaptive narrowband damping control for MMC, which first identifies single or multiple high-frequency resonances online by monitoring the behavior of oscillations associated with resonances, and subsequently suppress them by automatically configuring the multi-tuned narrowband damping control. In monitoring the oscillations, the IpDFT based spectral-peak detection algorithm and a resonance identification algorithm are proposed, ensuring accurate and robust estimations of the resonance frequencies. Consequently, the MMC can adaptively utilize the multi-tuned narrowband damping control to resolve detected high-frequency resonance issues during its integration into ac systems, without the need for a priori knowledge of the resonance frequencies. Furthermore, by continuously monitoring the system resonance conditions, the level of damping introduced by the multi-tuned damping control, as well as the width of the damping bands, are dynamically determined and adjusted. To guarantee the robustness of the adaptive damping control under varying grid conditions and changing operating conditions, an adaptive rule is also proposed to identify disappeared resonances and subsequently deactivate the corresponding damping controls.

EMT simulations demonstrate the effectiveness of the proposed adaptive damping control method across three MMC-based applications, with each application representing a practical resonance issue that has proven challenging to address. When compared with other existing works, the proposed narrowband damping method exhibits better performance in terms of:

- Accuracy and robustness of detection, for example, the immunity to transients and other disturbance signals;
- Capability to recognize changes in resonance conditions (e.g., whether they are diminishing or persisting);

- Ability to mitigate multiple high-frequency resonances existing concurrently;
- Adaptive regulation of the degree of damping introduced by multi-tuned damping control and the width of the damping band.

Several considerations must be taken into account when implementing the proposed adaptive damping control:

- The speed and accuracy of resonance detection are greatly influenced by, and somewhat limited by, the chosen window length (N) and the overlap size of the windows (N_{hop}) in the short-time Fourier transform. When resonances diverge rapidly, improper selection of N and N_{hop} could result in detection latency, compromised damping performance, or even system instability. This is because a diverging resonance could change the resonance conditions or initiate a system trip before the resonance is detected.
- The adaption rule fro damping gain tuning utilizes a static function (refer to (11)). The speed of this function is constrained by the updating rate of spectral analysis and the set-up of the static function parameters. Future research could address this, potentially by incorporating a Proportional-Integral compensator to regulate the damping gains of multi-tuned narrowband damper.
- The proposed adaptive control method presumes that the high-frequency impedance model of the MMC remains unchanged during operation, based on the assumption of a fixed control mode during operation. Further work should consider the adaption rule to accommodate changes in the MMC impedance due to variations in MMC control modes (Note: impedance of MMC with difference control modes can be found in [2]).

REFERENCES

[1] L. Harnefors, "Proof and application of the positive-net-damping stability criterion," *IEEE Transactions on Power Systems*, vol. 26, pp. 481–482, February 2011.

[2] P. Huang and L. Vanfretti, "Multi-tuned narrowband damping for suppressing MMC high-frequency oscillations," *IEEE Transactions on Power Delivery*, pp. 1–16, 2023.

[3] T. Messo, R. Luhtala, T. Roinila, D. Yang, X. Wang, and F. Blaabjerg, "Real-time impedance-based stability assessment of grid converter interactions," in *2017 IEEE 18th Workshop on Control and Modeling for Power Electronics (COMPEL)*, pp. 1–8, 2017.

[4] C. Zou and *et al.*, "Analysis of resonance between a VSC-HVDC converter and the ac grid," *IEEE Transactions on Power Electronics*, vol. 33, pp. 10157–10168, February 2018.

[5] P. Huang and L. Vanfretti, "Adaptive passivity compensation of grid-following mmc for stable grid integration," in *2022 IEEE Industry Applications Society Annual Meeting (IAS)*, pp. 1–8, 2022.

[6] I. Vieto, P. Huang, and *et al.*, "Online measurement of offshore wind farm impedance for adaptive control of HVDC transmission systems," in *2019 20th Workshop on Control and Modeling for Power Electronics (COMPEL)*, pp. 1–8, IEEE, 2019.

[7] W. Cao, Y. Ma, and F. Wang, "Adaptive impedance compensation of inverters for stable grid integration based on online resonance detection," in *2019 IEEE Applied Power Electronics Conference and Exposition (APEC)*, pp. 3151–3158, IEEE, 2019.

[8] J. Man, L. Chen, V. Terzija, and X. Xie, "Mitigating high-frequency resonance in MMC-HVDC systems using adaptive notch filters," *IEEE Transactions on Power Systems*, pp. 1–1, 2021.

[9] D. Agrež, "Weighted multipoint interpolated DFT to improve amplitude estimation of multifrequency signal," *IEEE Transactions on Instrumentation and Measurement*, vol. 51, pp. 287–292, April 2002.

[10] P. Romano and M. Paolone, "Enhanced interpolated-DFT for synchrophasor estimation in FPGAs: Theory, implementation, and validation of a PMU prototype," *IEEE Transactions on Instrumentation and Measurement*, vol. 63, no. 12, pp. 2824–2836, 2014.

[11] L. Jia, X. Ruan, W. Zhao, Z. Lin, and X. Wang, "An adaptive active damper for improving the stability of grid-connected inverters under weak grid," *IEEE Transactions on Power Electronics*, vol. 33, no. 11, pp. 9561–9574, 2018.

[12] T.-L. Lee, Y.-C. Wang, J.-C. Li, and J. M. Guerrero, "Hybrid active filter with variable conductance for harmonic resonance suppression in industrial power systems," *IEEE Transactions on Industrial Electronics*, vol. 62, no. 2, pp. 746–756, 2015.

[13] H. Wu and X. Wang, "Virtual-flux-based passivation of current control for grid-connected VSCs," *IEEE Transactions on Power Electronics*, vol. 35, pp. 12673–12677, December 2020.

[14] H. Wu, X. Wang, u. H. Kocewiak, J. Hjerrild, and M. Kazem, "Passivity-based harmonic stability analysis of an offshore wind farm connected to a mmc-hvdc," in *18th Wind Integration Workshop*, pp. 1–8, 2019.

[15] G. Stamatiou and M. Bongiorno, "Stability analysis of two-terminal vsc-hvdc systems using the net-damping criterion," *IEEE Transactions on Power Delivery*, vol. 31, no. 4, pp. 1748–1756, 2016.

[16] J. O. Smith, *Spectral Audio Signal Processing*. New York, NY, USA: W3K, 4th ed., 2011.

[17] "IEEE recommended practice for monitoring electric power quality,," *IEEE Std 1159-2019 (Revision of IEEE Std 1159-2009)*, pp. 1–98, 2019.

[18] W. S. Meyer and H. W. Dommel, "Numerical modelling of frequency-dependent transmission-line parameters in an electromagnetic transients program," *IEEE Transactions on Power Apparatus and Systems*, vol. PAS-93, no. 5, pp. 1401–1409, 1974.

Pengxiang Huang (S'21) received the B.S. degree from the Shanghai University of Electric Power, Shanghai, China, and the M.S. degree from George Washington University, Washington, DC, USA, all in electrical engineering. He is currently working toward the Ph.D. degree in electrical engineering at Rensselaer Polytechnic Institute, Troy, NY, USA.

His current interests are in renewable energy integration, flexible ac transmission system and MMC-based HVDC systems

Luigi Vanfretti Luigi Vanfretti (Senior Member, IEEE) was born in Guatemala and obtained his Engineering Degree with a concentration in Electrical Power in 2005 from Universidad de San Carlos de Guatemala. He then received the M.Sc. and Ph.D. degrees in electric power engineering from the Rensselaer Polytechnic Institute (RPI), Troy, NY, USA, in 2007 and 2009, respectively. He held postdoctoral research posts both at RPI and KTH Royal Institute of Technology, Sweden, in 2010.

He is currently a Full Professor at Rensselaer Polytechnic Institute, since July 2022, where he was a tenured Associate Professor from 2017-6/2022-6. At RPI, he leads research projects in his laboratory and with his research team, ALSETLab, in the domains of electrical power systems and aircraft electrification.